This article has been accepted for publication in a future issue of this journal, but has not been fully edited. Content may change prior to final publication. Citation information: DOI 10.1109/JPHOT.2016.2611441, IEEE Photonics Journal

A Positioning System for Photodiode Device Using Collocated LEDs

Samer Said Saab, Jr.[1] and Kaled Kamal Saab[2]

Abstract— **This paper proposes a novel light-emitting diode (LED) based system that can estimate the three-dimensional position of an object from the measurements of received signal strength (RSS). This work presents an alternative and relatively cheap approach for remotely estimating the location of an object. Unlike other LED based positioning systems, the proposed method employs a single base station (BS) including few LEDs with different orientations. In addition, the proposed system does not require a ceiling where the positioning LEDS are installed on. To illustrate the performance capabilities of the proposed system, we support our scheme analytically and numerically.**

Index Terms—Positioning system; visible light communications; light-emitting diode; received signal strength

I. Introduction

Unlike outdoor positioning using Global Navigation Satellite System (GNSS), indoor or even urban positioning uses different technologies, such as ultrawideband and inertial measurements, wide-angle cameras, wireless local area network (WLAN), and others fuse different technologies such as inertial sensors, radio frequency identification (RFID), light detection and raging, WLAN, odometry, and floor maps [1]. There exist several different methods for indoor and urban positioning, yet two alternatives seem to be most popular; namely radio frequencies (RF) and optic-based technologies (e.g., see [2]-[3]). RF technologies can be based on RFID (e.g., see [4]-[5]), WLAN (e.g., see [6]-[7]) hybrid WLAN-RFID (e.g., see [8]) or LIDAR (e.g., see [9]). RF-based systems suffer inevitable electromagnetic interference and multipath fading [10]. In addition, RF-based approaches deliver accuracies measured in meters, making them a poor fit for many applications (e.g., see [4]-[8]).

Visible light communication (VLC) seems to prove itself to be more accurate, in fact accurate between couple centimeters and tens of centimeters, depending on the dimensions of the room, light detector sizes, light-source position etc. The VLC methods may use either fluorescent lamps or LEDs as sources. LED can flicker at a high frequency, which may be manipulated to communicate certain messages, such as the exact angle it is at when pointing in a certain direction. In other words, the high switching speed of LEDs allows not only using single-state lamps for lighting, but creating a transmission channel as well. This offers a low cost system, medium to high communication speed, and no electromagnetic interference [11]-[12].

One common VLC positioning technique is based on triangulation, which consists of two methods: lateration and angulation. Lateration methods estimate the target location by measuring its distances from multiple reference points whereas angulation, measure angles relative to several reference points. Ranging techniques, needed for lateration, can be based on RSS; e.g., see [2] and the references therein, time of arrival (TOA), time difference of arrival (TDOA), or phase difference of arrival (PDOA). However, for systems based on TOA, TDOA or PDO, perfect synchronization among the clocks of transmitter and receiver has been assumed [13]. Exploiting the narrow field of view of LEDs to extract angle-of-arrival-based indoor localization, a multi-anchor multi-element VLC system is proposed [14]. The method used in [2] is a cheap and easy to employ method which uses RSS-based triangulation, with no need of synchronization among transmitters. The method of using mixed VLC-ultrasound location is proposed in [12], which considers a room with distributed LED lamps each with associated with an ultrasound receiver. However, this is limited by the time delay associated with the ultrasound propagation. Various techniques are integrated with VLC, such as time division multiplexing (TDM), in which every light source (or LED) is given a time slot in order to transmit signals at specific time to avoid overlapping signals. The method of TDM is tackled in [15], in which the method proposed considers a multiple access scheme of light positioning system applied to an indoor environment with numerous LEDs. Based on Cramer–Rao bound, [16] calculated the theoretical accuracy limitation of a class of RSS-based VLC systems. An RSS-based VLC indoor positioning is presented [17] with a multi-photo-detector target device, which can significantly reduce the number of LEDs installed on a ceiling. In particular, it is shown that positioning can be achieved provided that the total number of LEDs and photo-detectors is no smaller than four.

This paper proposes an alternative and relatively cheap RSS-based approach for remotely estimating the 3D location of an object without using a lighting grid or requiring a certain ceiling height. The proposed approach does not require numerous LEDs to be installed at different locations; rather it requires a single BS, not necessarily installed on a ceiling, facing the mobile station (MS) or the object to be localized. The BS includes few LED bulbs each situated at a different angle and one photo-detector mounted on the target object. Instead of having the LEDs

[1] S. S. Saab, Jr., Department of Electrical and Computer Engineering, Pennsylvania State University. Email: sys5880@psu.edu
[2] K. K. Saab, Department of Electrical and Computer Engineering, Georgia Institute of Technology. Email: ksaab3@gatech.edu

This article has been accepted for publication in a future issue of this journal, but has not been fully edited. Content may change prior to final publication. Citation information: DOI 10.1109/JPHOT.2016.2611441, IEEE Photonics Journal

transmission direction downward, the proposed method entails lateral transmission. Many applications can be envisaged where LEDs in a ceiling is not a part of the existing infrastructure. Such applications could relate to robotics with object grasping and manipulation including heavy autonomous forklift truck, where collocated LEDs can be installed on mobile vehicles and light sensors installed on target objects. Other applications include localization and navigation of cars inside a low ceiling parking building where GNSS coverage is uncertain. To the knowledge of the authors, no such approach has been proposed in the literature. The proposed setup is supported analytically and tested numerically.

The rest of the paper is organized as follows. Section II describes the proposed VLC system, presents the positioning concept, and formulates the problem under consideration. Error analyses are presented in Section III, followed by simulation examples in Section IV. The paper ends with conclusions and future work.

II. System Descriptions and Problem Formulation

This section presents the proposed system setup, the RSS model, and noise model adopted in this work. It also includes the concept of the localization scheme and presents the statement of a problem under consideration.

A. Proposed system setup

The LED sources, used for positioning, are collocated in a BS and oriented at different angles as depicted in Fig. 1 with notations of relevant variables listed in Table 1. The MS coordinates (d, ψ, φ) is considered as a class of spherical coordinates. The BS is placed higher than the MSs or the objects needed to be located so that the line of sight between LED and object domain is not obstructed by other MSs.

TABLE 1. MS COORDINATES AND LED ORIENTATION WITH BS AT THE ORIGIN

d	Radial distance between BS and MS
ψ	Azimuthal angle of MS in the *x*-*y* plane from the *x*-axis
φ	Elevation angle of MS is the angle between the line joining MS to origin and the projection of MS on the *z*-axis
Ψ_i	Orientation or azimuthal angle of the i^{th} LED in the *x*-*y* plane from the *x*-axis
Υ_i	Elevation angle of the i^{th} LED from *x*-*y* plane
α	Angle of irradiance
β	Angle of incidence

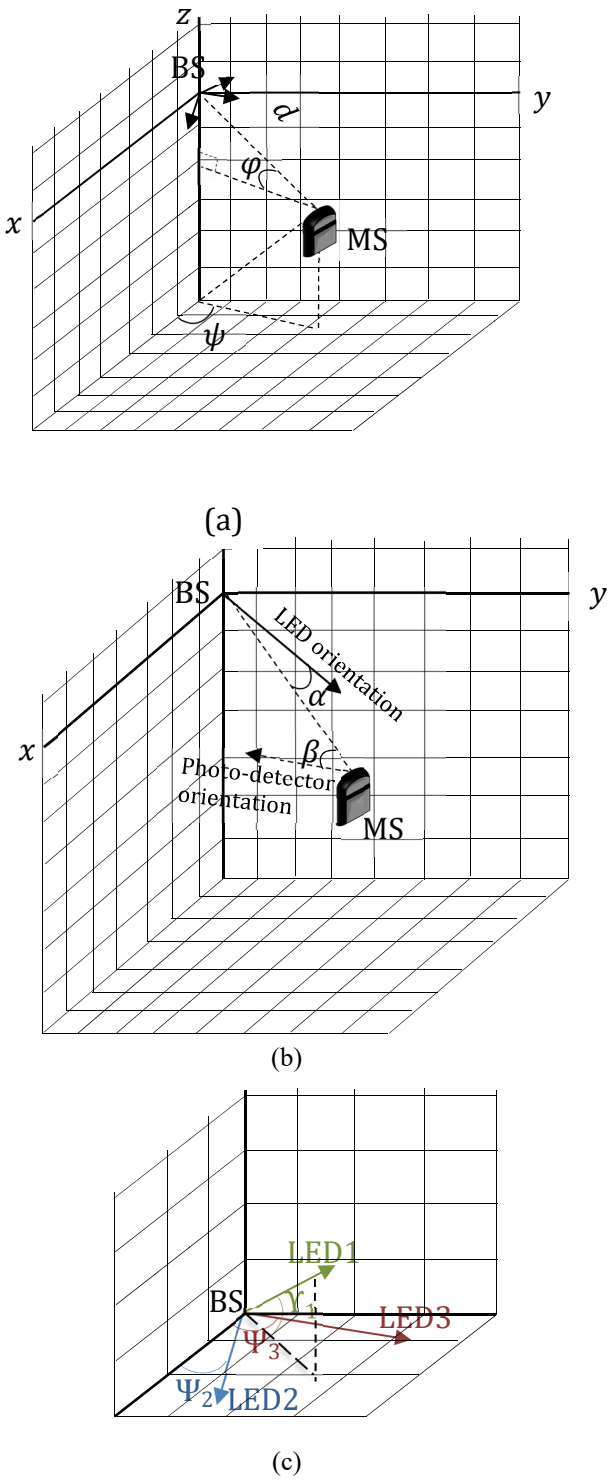

Fig. 1. (a) Environment of the three-dimensional positioning system; (b) angle of irradiance, α, and angle of incidence, β; (c) proposed multiple tilted LEDs structure, where the arrows indicate LEDs greatest illumination orientations. LEDS orientations: LED1 (Ψ_1, Υ_1); LED2 $(\Psi_2, \Upsilon_2 = 0)$; and LED3 $(\Psi_3, \Upsilon_3 = 0)$.

This article has been accepted for publication in a future issue of this journal, but has not been fully edited. Content may change prior to final publication. Citation information: DOI 10.1109/JPHOT.2016.2611441, IEEE Photonics Journal

In this study, we assume that:

(A1) The LED transmission is synchronized. That is, in order to avoid overlapping of light emitted from LEDs, the LEDs turns on and off sequentially at a rate, f_s.

(A2) The height of the photo-detector placed on each MS is assumed to be known to the MS positioning algorithm.

(A3) Each of the LED bulbs transmits its position and orientation, modulated in on-off-keying (OOK) format.

It is important to note that (A2) is a common explicit or implicit assumption used in the relevant literature (see; e.g., [2], [15], [16] and [17]). For example, in the case where the target device is a vehicle, then the photo-detector can be mounted on the vehicle at a specific height.

Remark 1: If the flickering rate, f_s, is sufficiently high, then the light transmitted by the different LEDs may appear steady to the human eye.

Remark 2: In case where the MS trajectory may include curves (e.g., navigation application); then a photo-detector could be installed on each side of the MS while considering a rectangular MS.

B. RSS model

In this study, we employ the power difference at the receiver side commonly adopted (see, e.g., [2] and [10]) given by

$$P_{rec}(d,\alpha,\beta) = \begin{cases} \frac{(m+1)AG}{2\pi d^2}\cos^m(\alpha)\cos(\beta)P_{diff}, & 0 \le \beta \le \beta_c \\ 0, & \beta > \beta_c \end{cases} \quad (1)$$

where m is the Lambertian order, G is a constant gain representing both the transmission gain of optical filter and the gain of optical concentrator, P_{diff} is the difference in transmitted power between logical 0s and 1s at the transmitter side. $P_{diff} = \eta_{OOK}P_{const}$, where η_{OOK} is the optical concentrator refractive index or modulation depth of the OOK modulator and P_{const} is the unmodulated optical power emitted from LED bulb. β is the angle of incidence with respect to the receiver axis, β_c is the concentrator field of view semi-angle, α is the angle of irradiance with respect to the transmitter perpendicular axis, and d is the distance between BS and MS. A is the physical area of photo-detector.

C. Noise Model:

For localization systems employing RSS, the noise is considered as a critical variable that directly affects the accuracy of estimation. Relevant noise is usually the combination of a) thermal noise, b) shot noise from background radiation [18], c) shot noise from received signal, and d) shot noise from dark current [19]. However, the dominant components in such applications are thermal noise and shot noise from background radiation [16]. According to [18], the noise can be modeled as zero-mean Gaussian process. The variance of noise, denoted σ_n^2,

$$\sigma_n^2 = \sigma_{shot}^2 + \sigma_{thermal}^2 \quad (2)$$

The variance of shot noise is given by

$$\sigma_{shot}^2 = 2q\gamma(P_{rec}(.))B + 2qI_{bg}I_2B \quad (3)$$

where q is the charge of an electron, B is the noise bandwidth, I_{bg} is the background current, which varies according to direct or indirect sunlight exposure, γ is the conversion efficiency also referred to as the photodiode responsivity [20], and for rectangular pulse shapes (e.g., OOK format), I_2 = 0.562, is the noise bandwidth factor, which is only a function of the transmitter pulse and equalized pulse shape and is independent of bit rate [20]. Since a field-effect transistor (FET) is used, more error is expected, due to current leakage and noise. The variance of thermal noise is

$$\sigma_{thermal}^2 = \frac{8\pi kT_k}{G_o}\eta AI_2B^2 + \frac{16\pi^2kT_k\Gamma}{g_m}\eta^2A^2I_3B^3 \quad (4)$$

where k is Boltzmann's constant, T_k is the absolute temperature, G_o is the open loop voltage gain, η is the fixed capacitance of the photo-detector per unit area, Γ is the FET channel noise factor, g_m is the FET transconductance, and the noise bandwidth factor, $I_3 = 0.0868$.

D. Positioning Concept and problem statement

We first establish a relation between the angle of irradiance and both LED and MS photo-detector orientations.

Claim 1. Assume the orientation vector of the LED is presented by (a,b,c) and the position vector of the MS by (x,y,z). Then we have,

$$\cos(\alpha) = \cos(\varphi)\cos(\Upsilon)\cos(\psi-\Psi) + \sin(\varphi)\sin(\Upsilon)$$

Proof. From the law of cosines, we have $\cos(\alpha) = \frac{ax+by+cz}{\|\text{LED}\|d}$ where $\|\text{LED}\| \triangleq \sqrt{a^2+b^2+c^2}$ and $d \triangleq \sqrt{x^2+y^2+z^2}$. We have

$$\begin{bmatrix} a \\ b \\ c \end{bmatrix} = \|\text{LED}\| \begin{bmatrix} \cos(\Psi)\cos(\Upsilon) \\ \sin(\Psi)\cos(\Upsilon) \\ \sin(\Upsilon) \end{bmatrix} \text{ and } \begin{bmatrix} x \\ y \\ z \end{bmatrix} = d \begin{bmatrix} \cos(\varphi)\cos(\psi) \\ \cos(\varphi)\sin(\psi) \\ \sin(\varphi) \end{bmatrix} \quad (5)$$

Thus, $\frac{ax+by+cz}{\|\text{LED}\|d} = \cos(\varphi)\cos(\Upsilon)\cos(\psi-\Psi) + \sin(\varphi)\sin(\Upsilon)$ ■

Based on Claim 1 and for $\beta \le \beta_c$, the power difference at the receiver side (1) or RSS can be presented as

$$P_{rec}(d,\beta,\varphi,\psi) = \mathrm{C}\frac{\cos(\beta)}{d^2}[\cos(\varphi)\cos(\Upsilon)\cos(\psi-\Psi) + \sin(\varphi)\sin(\Upsilon)]^m \quad (6)$$

where $\mathrm{C} \triangleq \frac{AG(m+1)}{2\pi}P_{diff}$. RSS (6) is considered as a nonlinear function of the 3D MS coordinates (d,ψ,φ), and angle of incidence, β. It is important to note that, unlike (ψ,φ), the coupling of $\frac{\cos(\beta)}{d^2}$ is independent of LED orientation. Consequently, one RSS measure results in one equation with three unknowns, namely, $\left(\frac{\cos(\beta)}{d^2},\psi,\varphi\right)$. Therefore, at least three LEDs with different orientations are

This article has been accepted for publication in a future issue of this journal, but has not been fully edited. Content may change prior to final publication. Citation information: DOI 10.1109/JPHOT.2016.2611441, IEEE Photonics Journal

required to estimate $\left(\frac{\cos(\beta)}{d^2}, \psi, \varphi\right)$. However, since the height of the photo-detector, z, is known to the MS, then we have $z = d\sin(\varphi)$. Consequently, d can be estimated from the knowledge of z and the estimate of φ, and the 3D location of MS can be obtained from (5). In addition, angle of incidence, $\beta = cos^{-1}(\frac{\cos(\beta)}{d^2}d^2)$, can be estimated from the estimate of $\frac{\cos(\beta)}{d^2}$ and estimate of d. By using measurements of three LEDs with different orientations, the 3D location of MS along with angle of incidence can be estimated. However, due to errors in RSS measurements, deployment of more than three LEDs should improve instantaneous positioning estimate as well as coverage area. Therefore, the MS location can be obtained by directly solving such nonlinear equations in presence of measurement errors using one of the existing renowned iterative techniques. Once the MS location is estimated with respect to BS, then its position estimate can be evaluated.

Remark 3: If the photo-detector placed on each MS were assumed to be shaped like a half-sphere shell and placed below BS, then the effective area of the photo-detector would appear to be the same at any position in the spatial domain and the angle of incidence, β, would become negligible. Consequently, the coupling issue of $\frac{\cos(\beta)}{d^2}$ would no longer hold since $\beta = 0$ and assumption (A2) would not be needed.

Problem Statement: Based on the system setup under consideration, assumptions (A1)-(A3), and erroneous RSS measurements, provide an analytical statistical error for the MS position estimate as well as angle of incidence.

III. Error Analysis

This section provides statistical position error estimates of the proposed system. The proposed localization algorithm first estimates the triplet $\left(\xi \triangleq \frac{\cos(\beta)}{d^2}, \psi, \varphi\right)$, then estimates d from the estimate φ and knowledge of the photo-detector height, and subsequently it estimates β from the estimates of ξ and d. We first study the statistical errors of (ξ, ψ, φ) due to noise. The errors are denoted by $(\delta\xi, \delta\psi, \delta\varphi)$. Consider RSS model corresponding to the i^{th} LED with orientation (Ψ_i, Υ_i), with $1 \le i \le N$, then (6) leads to

$$P_{rec,i}(\xi, \varphi, \psi) = \mathrm{C}\xi\cos^m(\alpha_i) \tag{7}$$

where $\cos(\alpha_i) = \cos(\varphi)\cos(\Upsilon_i)\cos(\psi - \Psi_i) + \sin(\varphi)\sin(\Upsilon_i)$. Using Taylor series expansion while dropping the second-order terms and higher, we obtain

$$P_{rec,i}(\xi + \delta\xi, \psi + \delta\psi, \varphi + \delta\varphi) \cong P_{rec,i}(\xi, \varphi, \psi) + J_{i,1}\delta\xi + J_{i,2}\delta\psi + J_{i,3}\delta\varphi \tag{8}$$

where $J_{i,1} = \mathrm{C}\cos^m(\alpha_i)$

$$J_{i,2} = -\mathrm{C}\xi m\cos^{m-1}(\alpha_i)\cos(\varphi)\cos(\Upsilon_i)\sin(\psi - \Psi_i)$$

$$J_{i,3} = \mathrm{C}\xi m\cos^{m-1}(\alpha_i)[-\sin(\varphi)\cos(\Upsilon_i)\cos(\psi - \Psi_i) + \cos(\varphi)\sin(\Upsilon_i)]$$

It is important to note that $J_{i,j}, 1 \le i \le N, 1 \le j \le 3$ are the elements of the Jacobian matrix associated with (7). Let

$$n_i \triangleq P_{rec,i}(d + \delta d, \psi + \Psi_i + \delta\psi, \varphi + \Upsilon_i + \delta\varphi) - P_{rec,i}(d, \psi + \Psi_i, \varphi + \Upsilon_i)$$

represent the RSS measurement error due to noise of the i^{th} LED. Let $n \triangleq \{n_i\} \in \Re^N$. Consequently, (8) implies

$$n = J\begin{bmatrix}\delta\xi \\ \delta\psi \\ \delta\varphi\end{bmatrix} \tag{9}$$

Assuming that J is full-column rank, we multiply both sides of (9) by J^{-1} whenever $i = 3$ or by Moore–Penrose pseudoinverse of J, $J^{\dagger} = [J^T J]^{-1}J^T$ whenever $i > 3$, to obtain an expression for the error vector, δL

$$\delta L \triangleq \begin{bmatrix}\delta\xi \\ \delta\psi \\ \delta\varphi\end{bmatrix} = \begin{cases}J^{-1}n, & i = 3 \\ J^{\dagger}n, & i > 3\end{cases} \tag{10}$$

Consequently, the covariance of δL, is given by $P \triangleq E\{\delta L\delta L^T\} = J^{-1}E\{nn^T\}J^{-1^T}$ or $P = J^{\dagger}E\{nn^T\}J^{\dagger^T}$, where $E\{.\}$ is the expectation operator. Since the associated RSS measurement errors can be assumed white noise, then $R \triangleq E\{nn^T\} \in \mathbb{R}^{N\times N}$ is a diagonal matrix with diagonal entries $(\sigma_n^2)_i, 1 \le i \le N$, where $(\sigma_n^2)_i$ corresponds to the noise variance associated with the i^{th} LED. Therefore,

$$P = E\{\delta L\delta L^T\} = \begin{cases}J^{-1}RJ^{-1^T}, & i = 3 \\ J^{\dagger}RJ^{\dagger^T}, & i > 3\end{cases} \tag{11}$$

The error variances, $E[\delta\xi\delta\xi^T]$, $E[\delta\psi\delta\psi^T]$, and $E[\delta\varphi\delta\varphi^T]$ can be extracted from the first second, and third diagonal entries of P, respectively. Based on the knowledge of the heights of MS and BS, the z-coordinate of MS, z, is evaluated where $z = d\sin(\varphi)$ or $d = \frac{z}{\sin(\varphi)}, \varphi \ne 0$. Thus, $\delta d \cong -z\frac{\cos(\varphi)}{\sin^2(\varphi)}\delta\varphi$ and $E[\delta d^2] \cong \left(z\frac{\cos(\varphi)}{\sin^2(\varphi)}\right)^2 E[\delta\varphi^2]$ or

$$E[\delta d^2] \cong \left(\frac{d}{\tan(\varphi)}\right)^2 E[\delta\varphi^2] \tag{12}$$

Moreover, $\xi = \frac{\cos(\beta)}{d^2}, d \ne 0$ or $\beta = \cos^{-1}(\xi d^2)$. Therefore, $\delta\beta \cong \frac{-1}{\sqrt{1-(\xi d^2)^2}}\{2\xi d\delta d + d^2\delta\xi\}$. Substituting $\delta d \cong -z\frac{\cos(\varphi)}{\sin^2(\varphi)}\delta\varphi$ in $\delta\beta$, we obtain $\delta\beta \cong \Gamma\delta L$, where $\Gamma \triangleq \frac{1}{\sqrt{1-\left(\xi d^2\right)^2}}\left[-d^2 \quad 0 \quad 2\xi dz\frac{\cos(\varphi)}{\sin^2(\varphi)}\right]$. Consequently,

$$E[\delta\beta^2] = \Gamma P\Gamma^T \tag{13}$$

The statistical error models given by (11)-(13) cover all relevant variables.

This article has been accepted for publication in a future issue of this journal, but has not been fully edited. Content may change prior to final publication. Citation information: DOI 10.1109/JPHOT.2016.2611441, IEEE Photonics Journal

IV. Numerical Results

In this example we fix the photo-detector orientation vector to $[-1 \quad 0 \quad 0]$ for all MS positions. However, the corresponding incident angles vary for different MS positions. Newton-Raphson is employed to estimate the MS spherical coordinates as presented in Table 1 with same initial guess, at (0.006, 0.14, −0.1), for all MS locations throughout this example. Subsequently, the Cartesian coordinates are extracted. MATLAB is employed for all simulations. Table 2 lists the parameters, similar to those in [2], pertaining to RSS model (1) and noise model (3) and (4); where, $T_s(\beta)$ is the gain of optical filter, η_c is the refractive index of optical concentrator, η_{OOK} is the optical concentrator refractive index, and γ is the conversion efficiency. We consider two scenarios for the noise, namely with direct sunlight exposure (DSE) and indirect sunlight exposure (ISE).

TABLE 2. PARAMETERS EMPLOYED IN SIMULATIONS

LED	Thermal Noise	Shot Noise
$T_s(\beta) = 1.0$	$T_K = 295$K	B = 640 KHz
$G = 2.548$	$G_o = 10$	$I_2 = 0.562$
$\eta_c = 1.5$	$I_3 = 0.0868$	DSE: $I_{bg-dir} = 5100$ μA
$\eta_{OOK} = 12.5\%$	$g_m = 30$mS	ISE: $I_{bg-ind} = 740$μA
$P_{LED} = 16$ W	$\Gamma = 1.5$	
$\gamma = 0.54$ A/W	$\eta = 112$ pF/cm^2	

We first examine the coverage of the proposed system under DSE for different values of Lambertian orders while considering two different LEDs setups. In particular, Fig. 2 shows the coverage using three LEDs while Fig. 3 uses six LEDs. It can be noticed as the Lambertian order, m, is increased smaller and tighter coverage is attained; however, better accuracy is achieved for further distances facing BS.

Remark 4: This remark explains the unpredictability in the results for $m > 1$. The function part in which the RSS model (1) depends on m is $f(m,\alpha) \triangleq (m+1)\cos^m(\alpha)$. For a fixed position of MS, the corresponding value of RSS increases as $f(m,\alpha)$ increases and $f(m,\alpha)$ is not a monotonic function with respect to m. For example, $f(m=1,\alpha=60^o) > f(m=4,\alpha=60^o)$ yet $f(m=1,\alpha=30^o) < f(m=4,\alpha=30^o)$. In general and in presence of noise, a better position estimate is expected for larger values of RSS. Consequently, one may not conclude that the performance is always improved for smaller values of m. In order to further illustrate the results; e.g., of Fig. 2, we plot the RSS values (without noise) in Fig. 4 corresponding to LED with orientation $(\Psi,\Upsilon) = (0^o, 10^o)$, for different MS azimuth angles, ψ, for $d = 10$m and $d = 2$m. It is important to note that when $\psi = 0$, the MS is facing the LED. As ψ decreases the irradiance angle, α, decreases and RSS increases for both $d = 10$m and $d = 2$m. However, the RSS values corresponding to $m = 4$ and $d = 10$m are larger than the ones corresponding to $m = 1$ for $-40^o \lesssim \psi \lesssim 40^o$ yet the RSS values corresponding to $m = 4$ and $d = 2$ m are always smaller than the ones corresponding to $m = 1$.

While using only 3 LEDs, the coverage area, for $m = 1$ constraint to position error less than 30cm under DSE, is about 100 m^2, and 300 m^2 for position error less than 1m. Using more LEDs with different orientations increases the coverage as depicted in Fig. 3.

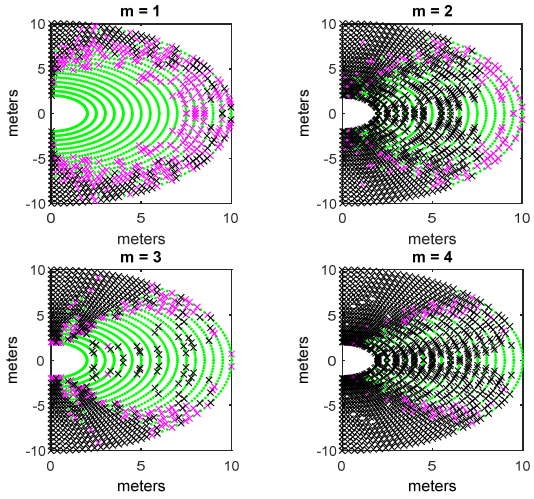

Fig. 2. Performance coverage for Lambertian orders, $1 \le m \le 4$, under DSE using 3 LEDs with orientations (Ψ,Υ): $(0^o, 10^o)$, $(-25^o, 0^o)$, and $(25^o, 0^o)$. The MS locations are described by: $2\text{m} \le d \le 10\text{m}$, $-90^o \le \psi \le 90^o$, and $z = -1.3$m. Photo-detector area, $A = 10\text{cm}^2$. The green dots correspond to MS location errors less 30cm, the cyan x-marks correspond to errors between 30cm and 1m, and the black x-marks correspond to location errors greater than 1m.

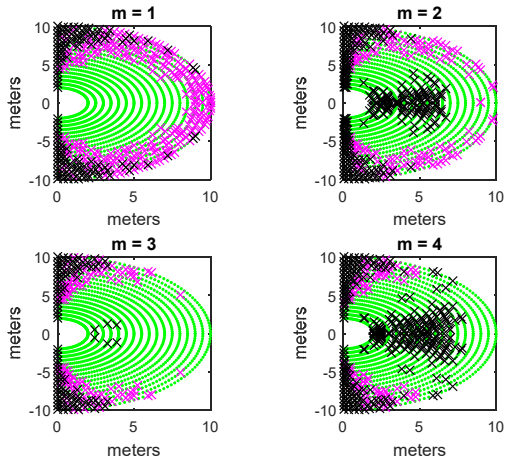

Fig. 3. Same setup as in Fig. 2 except for using 6 LEDs with orientations (Ψ,Υ): $(0^o, 0^o)$, $(0^o, 10^o)$, $(-25^o, 0^o)$, $(25^o, 0^o)$, $(-25^o, 10^o)$, and $(25^o, 10^o)$.

This article has been accepted for publication in a future issue of this journal, but has not been fully edited. Content may change prior to final publication. Citation information: DOI 10.1109/JPHOT.2016.2611441, IEEE Photonics Journal

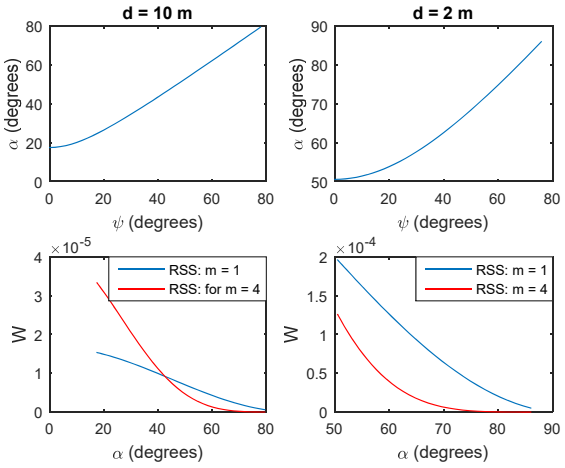

Fig. 4. α versus ψ (top plots) and RSS versus α (bottom plots) using 1 LED with orientations (Ψ, Υ): $(0^o, 10^o)$. $z = -1.3\text{m}$. Photo-detector area, $A = 10\text{cm}^2$. The left plots correspond to $d = 10\text{m}$ and the right plots correspond to $d = 2\text{m}$.

Fig. 5 shows the radial errors versus the MS x-y coordinates with $m = 1$. As expected the error increases as d and/or ψ increase since with $m = 1$ RSS (1) decreases as d and/or ψ increase. In order to further illustrate the performance of the proposed system we take different values of d, $2\text{m} \leq d \leq 10\text{m}$, and for each fixed value of d we vary ψ in the range $-60^o \leq \psi \leq 60^o$. Subsequently, we take the average of absolute radial error. In this study we use three and six collocated LEDs while considering ISE and DSE. The results are depicted in Fig. 6 for three LEDs and Fig. 7 for six LEDs. As elaborated in Remark 4, the errors are expected to fluctuate for the case where $m > 1$. Significant performance improvement is attained when 6 LEDs are used. In addition, better performance is achieved for $m = 3$ when $d \geq 8\text{m}$. However, the errors for $2\text{m} \leq d \leq 4\text{m}$ with $m = 1$, listed in Table 3, are relatively negligible. The maximum average errors are listed in Table 4.

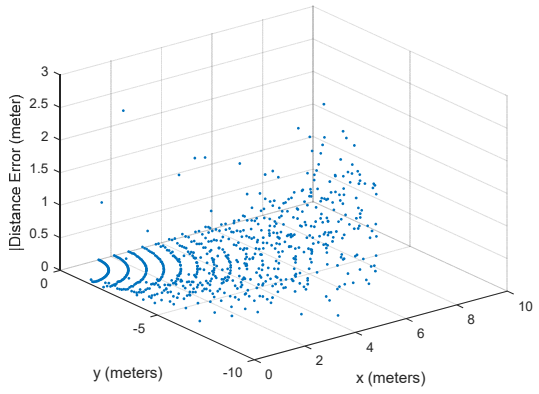

Fig. 5. Radial errors versus the MS x-y coordinates with system setup similar to the one employed in Fig. 2 but with $m = 1$.

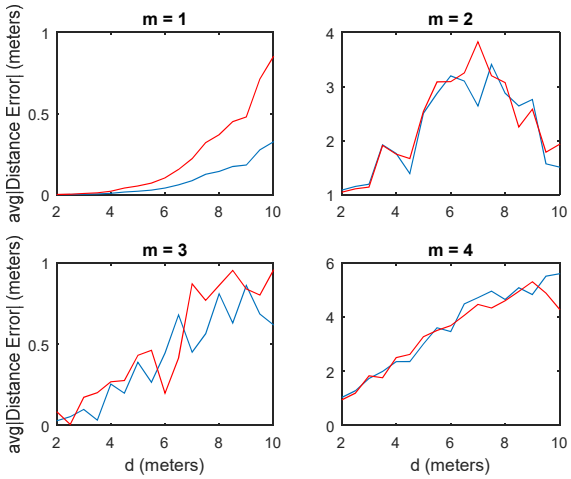

Fig. 6. $\text{AVG}_{-60^o \leq \psi \leq 60^o}|\text{RADIAL ERROR}|$ with 3 LEDs using the same setup as in Fig. 2. ISE plots in blue while DSE plots in red.

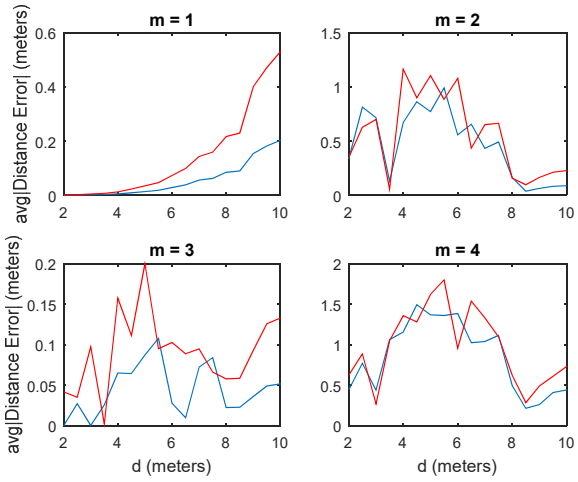

Fig. 7. $\text{AVG}_{-60^o \leq \psi \leq 60^o}|\text{RADIAL ERROR}|$ with 6 LEDs using the same setup as in Fig. 3. ISE plots in blue while DSE plots in red.

TABLE 3. $\text{AVG}_{-60^o \leq \psi \leq 60^o}|\text{RADIAL ERROR}|$ WITH $m = 1$

		$d = 2\text{m}$	$d = 3\text{m}$	$d = 4\text{m}$
3 LEDs	ISE	$5.1 \times 10^{-4}\text{m}$	$3.0 \times 10^{-3}\text{m}$	$8.6 \times 10^{-3}\text{m}$
	DSE	$1.3 \times 10^{-3}\text{m}$	$7.3 \times 10^{-3}\text{m}$	$2.2 \times 10^{-2}\text{m}$
6 LEDs	ISE	$3.5 \times 10^{-4}\text{m}$	$1.9 \times 10^{-3}\text{m}$	$5.0 \times 10^{-3}\text{m}$
	DSE	$8.4 \times 10^{-4}\text{m}$	$4.7 \times 10^{-3}\text{m}$	$1.3 \times 10^{-2}\text{m}$

This article has been accepted for publication in a future issue of this journal, but has not been fully edited. Content may change prior to final publication. Citation information: DOI 10.1109/JPHOT.2016.2611441, IEEE Photonics Journal

TABLE 4. $\text{MAX}_{2\text{m}\le d\le 10\text{m}}\ \text{AVG}_{-60^o\le\psi\le 60^o}|\text{RADIAL ERROR}|$

		$m=1$	$m=2$	$m=3$	$m=4$
3 LEDs	ISE	0.33m	3.4m	0.86m	5.6m
	DSE	0.85m	3.8m	0.96m	5.3m
6 LEDs	ISE	0.2m	0.99m	1.1m	1.49m
	DSE	0.53m	1.16m	2m	1.8m

In what follows we justify the analytical results provided in Section III as well as examining the performance capabilities of the proposed system in function of the variables d and ψ, and the parameters A and z. The performance depends on many different scenarios such as the number of LEDs under consideration and their orientations and different MS locations. The subsequent results are only based on relevant specific scenarios.

Fig. 8 shows an increase in errors as distance between the MS and BS is increased for $m=1$ using 6 LEDs under DSE while holding $\psi=0^o$ and $z=-1.3$ m. Specifically, $|\delta d|\cong 1$ cm at $d=5$ m and it increases to $|\delta d|\cong 1$ m at $d=15$ m. The MS orientation errors $|\delta\psi|$ and $|\delta\varphi|$ are within 1^o. Fig. 9 shows a sub-meter steadiness in position errors as the azimuth angle is varied, $-50^o\le\psi\le 50^o$, using 3 LEDs while holding $d=10$ m. Fig. 10 examines performance as the MS height is varied, $-3\text{ m}\le z\le -0.1\text{ m}$, while holding $d=10$m and $\psi=0^o$ under ISE with $m=2$ using 3 LEDs. In the following scenario, we use small value of $|\delta\Psi|=0.2^o$. As the height of the MS approaches the height of BS, the error in distance, $|\delta d|$, is increased. It is important to note that as height of the MS approaches the height of BS, $|\varphi|$ is decreased so is $|\tan(\varphi)|$. This phenomena is analytically reflected in (12). We also notice a slight decrease in $|\delta\psi|$ and $|\delta\varphi|$.

Fig. 8, Fig. 9 and Fig. 10 show $|\delta d|$, $|\delta\psi|$, $|\delta\varphi|$ and $|\delta\beta|$ along with their expected standard deviations extracted from (11)-(13), in function of d, ψ, and z, respectively; whereas Fig. 11 shows the position error versus the photo-detector area, A, under DSE and ISE. Based on numerical results, e.g. Fig. 8 to Fig. 10, the analytical results presented in (11)-(13) (in red) are rather representative of the actual errors (in blue). Fig. 11 shows the position errors in function of photo-detector area, $1\text{ cm}^2\le A\le 100\text{ cm}^2$, while considering both DSE and ISE using 6 LEDs with $d=10$m, $\psi=30^o$, and $z=-1.3$ m. It can be observed that the position error is approximately inversely proportional to A. Instead of using traditional Newton-Raphson method, future work can involve implementation of stochastic iterative methods (e.g., [21]) aiming at significantly reducing the impact of noise.

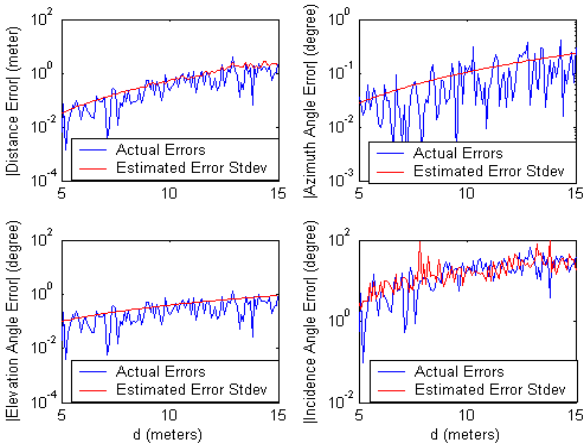

Fig. 8. Absolute errors (blue) along with their corresponding standard deviations (red) extracted from (11)-(13) associated with d (top left), ψ (top right), φ (bottom left) and β (bottom right); under DSE with $m=1$ using 6 LEDs with orientations (Ψ,Υ): $(0^o,0^o)$, $(0^o,10^o)$, $(-25^o,0^o)$, $(25^o,0^o)$, $(-25^o,10^o)$, and $(25^o,10^o)$. The MS locations are described by: 5 m $\le d\le$ 15 m, $\psi=0^o$, and $z=-1.3$ m. Photo-detector area, $A=10\text{ cm}^2$.

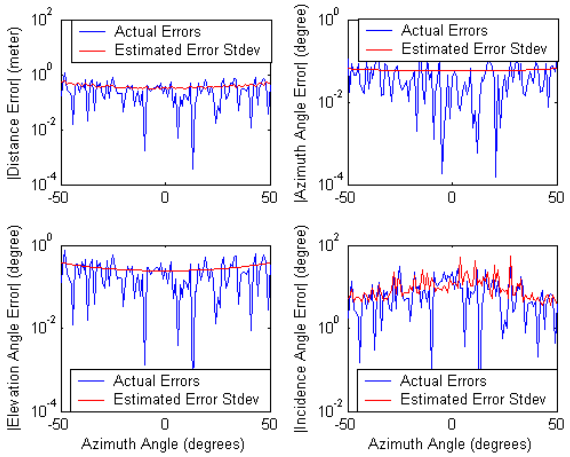

Fig. 9. Same as in Fig. 8 but with ISE, $m=1$ and using 3 LEDs with orientations (Ψ,Υ): $(0^o,10^o)$, $(-25^o,0^o)$, and $(25^o,0^o)$. The MS locations are described by: $d=10$m, $-50^o\le\psi\le 50^o$.

This article has been accepted for publication in a future issue of this journal, but has not been fully edited. Content may change prior to final publication. Citation information: DOI 10.1109/JPHOT.2016.2611441, IEEE Photonics Journal

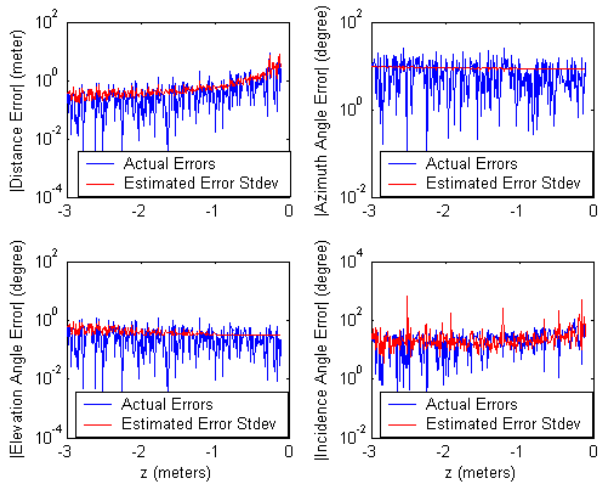

Fig. 10. Same as in Fig. 9 but with $m = 2$ and orientations (Ψ, Υ): $(0^o, 10^o)$, $(-0.2^o, 0^o)$, and $(0.2^o, 0^o)$. The MS locations are described by: $d = 10$m, $\psi = 0^o$, and -3 m $\leq z \leq -0.1$ m.

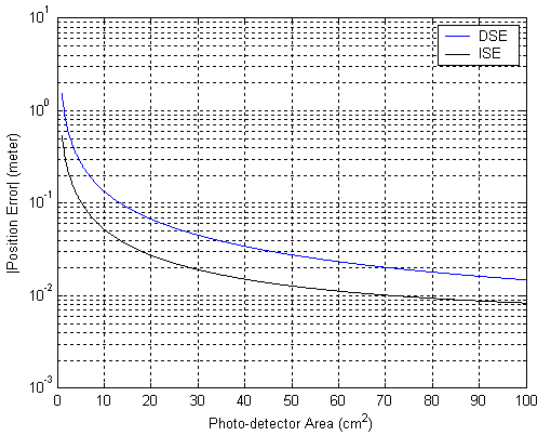

Fig. 11. Position errors in function of photo-detector area: 1 cm^2 $\leq A \leq$ 100 cm^2; with $m = 2$ using 6 LEDs with orientations (Ψ, Υ): $(0^o, 0^o)$, $(0^o, 10^o)$, $(-25^o, 0^o)$, $(25^o, 0^o)$, $(-25^o, 10^o)$, and $(25^o, 10^o)$. The MS location is described by: $d = 10$m, $\psi = 30^o$, and $z = -1.3$ m.

V. Conclusion and Future Work

This paper presented an alternative approach to positioning system setup based on visible light communication and RSS. The proposed approach does not require a ceiling or a grid of LEDs but instead it is based on a single BS consisting of three or more collocated LEDs with different orientations. In addition, unlike conventional schemes where light transmission is vertical, the proposed method allows horizontal transmission accommodating significantly longer ranges between LED and photo-detector. Consequently, the proposed setting can outspread the application domain of VLC-based positioning schemes to different scenarios such as localization and navigation of vehicles inside a low ceiling parking; and other class of applications involving robotic object grasping. A statistical error model was provided analytically and justified numerically. The performance was examined under different Lambertian orders, $1 \leq m \leq 4$. For ranges beyond 8 m, a Lambertian order of 3 using 6 LEDs provided better performance with a radial error less than 5 cm under ISE and 13 cm under DSE. However, for short ranges, $m = 1$ showed promising results (e.g., a sub-millimeter accuracy was achieved for $d = 2$ m). With a photo-detector area of 10 cm^2, sub-meter accuracy was achieved using six collocated LEDs under DSE in a 300 m^2 area.

Future work can involve (a) optimal LED orientations such that the positioning outages are minimized, and (b) implementation of such a system setup for navigation.

Acknowledgment

The authors would like to thank Professor Samer S. Saab, the anonymous reviewers and associate editor for their constructive comments and suggestions in improving this work.

References

[1] D. Dardari, P. Closas, P.M. Djuric, "Indoor tracking: theory, methods, and technologies," *IEEE Trans. Veh. Tech.,* vol. 64, no. 4, pp. 1263-1278, 2015.

[2] W. Zhang, M. S. Chowdhury, M. Kavehrad, "Asynchronous indoor positioning system based on visible light communications" *Optical Engineering*, vol. 53, no. 4, pp. 1-9, 2014.

[3] W. Gu, W. Zhang, J. Wang, A. Kashani, M. Kavehrad, "Three dimensional indoor positioning based on visible light with Gaussian mixture sigma-point particle filter technique," *SPIE OPTO.,* May 2015.

[4] S. S. Saab, Z. Nakad "A standalone RFID indoor positioning system using passive tags," *IEEE Trans. Ind. Electron.*, vol. 58, no. 5, pp. 24-40, May 2011.

[5] S. S. Saab and H. Msheik, "A Novel RFID Based Pose Estimation Using Single Stationary Antenna," *IEEE Trans. Ind. Electron.*, vol. 63, no. 3, pp. 1842-1852, 2016.

[6] A. Kushki, K.N. Plataniotis, A.N. Venetsanopoulos, "Kernel-based positioning in wireless local area networks," *IEEE Trans. Mobile Comp.*, vol. 6, no. 6, pp. 689-705, 2007.

[7] J. Talvitie, M. Renfors, E.S. Lohan, "Distance-based interpolation and extrapolation methods for RSS-based localization with indoor wireless signals," *IEEE Trans. Veh. Tech.,* vol. 64, no. 4, pp. 1340-1353, 2015.

[8] M. Hasani, J. Talvitie, L. Sydanheimo, E.-S. Lohan, L. Ukkonen, "Hybrid WLAN-RFID indoor localization solution utilizing textile tag," *IEEE Antenn. and Wireless Propag. Letters*, vol. 14, pp. 1358-1361, 2015.

[9] A. Y. Hata; D. F. Wolf, "Feature Detection for Vehicle Localization in Urban Environments Using a Multilayer LIDAR," *IEEE Trans. on Intellig. Transp. Syst.*, vol. 17, no. 3, pp. 420-429, 2016.

[10] J. Lim, "Ubiquitous 3D Positioning Systems by LED-Based Visible Light Communications" *IEEE Wireless Comm.* pp. 80-85, April, 2015

[11] W. Xu, M. Wu, H. Zhang, X.-H. You, and C. Zhao, "ACO-OFDM specified recoverable upper-clipping with efficient detection for optical wireless communications," *IEEE Photon. J.*, vol. 6, no. 5, pp. 1–17, 2014.

[12] I. Martin-Garcia, et al., "Indoor Location Technique Based on

Visible Light Communications and Ultrasound Emitters" *IEEE Int. Conf. on Consum. Electron.* pp. 297-298, 2015.

[13] T. Q. Wang, Y. A. Sekercioglu, A. Neild, and J. Armstrong. "Position accuracy of time-of-arrival based ranging using visible light with application in indoor localization systems," *J. Lightw. Technol*., vol. 31, no. 20, pp. 3302-3308, Oct. 2013.

[14] Y. S. Erogluy, I. Guvency, N. Palay and M. Yukselz, "AOA-based localization and tracking in multi-element VLC systems," IEEE 16th Annual Conf. on Wireless and Microwave Technology (WAMICON), pp. 1-5, Cocoa Beach, FL, 2015.

[15] Y. Hou, S. Xiao, H. Zheng, W. Hu, "Multiple Access Scheme Based on Block Encoding Time Division Multiplexing in an Indoor Positioning System Using Visible Light" *J. Opt. Commun. Netw.* vol. 7, no. 5, pp. 489-495, 2015.

[16] X. Zhang, J. Duan, Y. Fu, and A. Shi, "Theoretical accuracy analysis of indoor visible light communication positioning system based on received signal strength indicator," *J. Lightw. Technol.*, vol. 32, no. 21, pp. 4180-4186, Nov., 2014.

[17] W. Xu, J. Wang, H. Shen, H. Zhang, X. You, "Indoor Positioning for Multiphotodiode Device Using Visible-Light Communications," *IEEE Photon. J*., vol. 8, no. 1, pp. 1-11, 2016.

[18] T. Komine and M. Nakagawa, "Fundamental analysis for visible-light communication system using LED lights," *IEEE Trans. Consumer Electron*., vol. 50, no. 1, pp. 100–107, Feb. 2004.

[19] H. Manor and S. Arnon, "Performance of an optical wireless communication system as a function of wavelength," *Appl. Opt*., vol. 42, no. 21, pp. 4285–4294, Jul. 2003.

[20] M. Kavehrad, Z. Zhou, and M.S. Chowdhury. *Short Range Optical Wireless: Theory and Applications*. John Wiley & Sons, 2015.

[21] K. K. Saab and S. S. Saab, Jr, "A stochastic Newton's method with noisy function measurements", *IEEE Signal Process. Letters*, vol. 23, no. 3, pp. 361-365, 2016.